

# Dual Marching Cubes

Gregory M. Nielson

Arizona State University

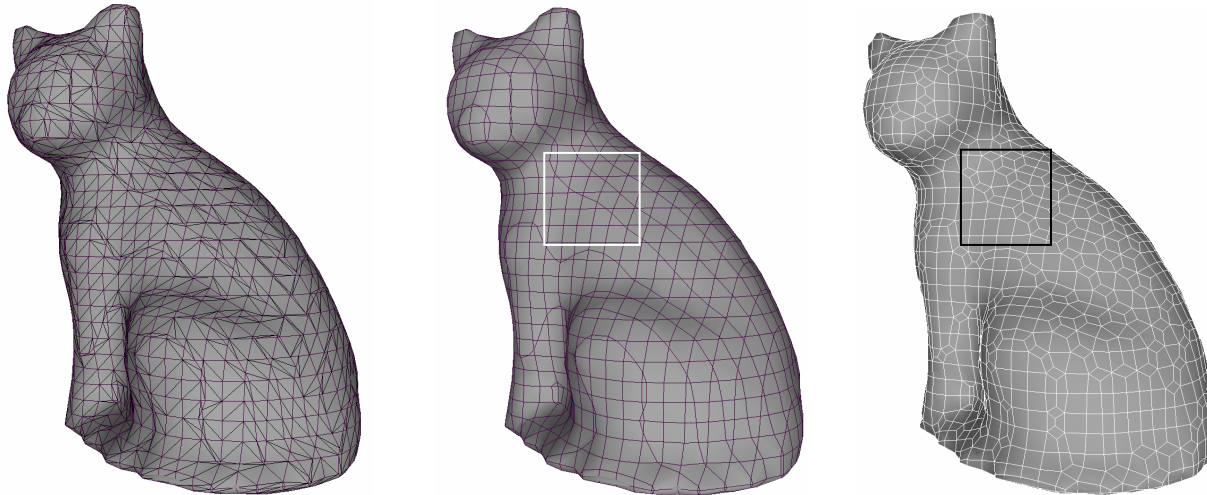


Figure 1. March Cubes Surface

MC-Patch surface,  $S$

MC-Dual surface,  $S^\diamond$

## ABSTRACT

We present the definition and computational algorithms for a new class of surfaces which are dual to the isosurface produced by the widely used marching cubes (MC) algorithm. These new isosurfaces have the same separating properties as the MC surfaces but they are comprised of quad patches that tend to eliminate the common negative aspect of poorly shaped triangles of the MC isosurfaces. Based upon the concept of this new dual operator, we describe a simple, but rather effective iterative scheme for producing smooth separating surfaces for binary, enumerated volumes which are often produced by segmentation algorithms. Both the dual surface algorithm and the iterative smoothing scheme are easily implemented.

**CR Categories and Subject Descriptors:** I.3.5 [Computer Graphics]: Computation Geometry and Object Modeling – Surface, solid and object representations

**Additional Keywords:** Marching Cubes, isosurfaces, triangular mesh, dual graph, segmented data, smoothing

## 1 INTRODUCTION

The marching cubes (MC) algorithm ( see [10], [11], [12] ) is a widely used technique for computing triangular mesh isosurfaces from discretely sampled volume data over rectilinear lattices. Here we introduce the concept of a dual surface. This dual surface tends to eliminate the poorly shaped triangles often

present in MC surfaces. In a nutshell, we obtain this dual surface in the following manner. First, we extend the concept of the MC surface to a patch version which eliminates the edges of the MC surface interior to voxels to obtain a surface,  $S$ , with polygon bounded patches where each vertex is included in exactly four patches. Then for each patch of  $S$  there is associated a vertex of the dual surface. The dual consists of quad patches which are connected in exactly the same manner as the connectivity of the vertices of the surface  $S$ . See Figures 1 and 2.

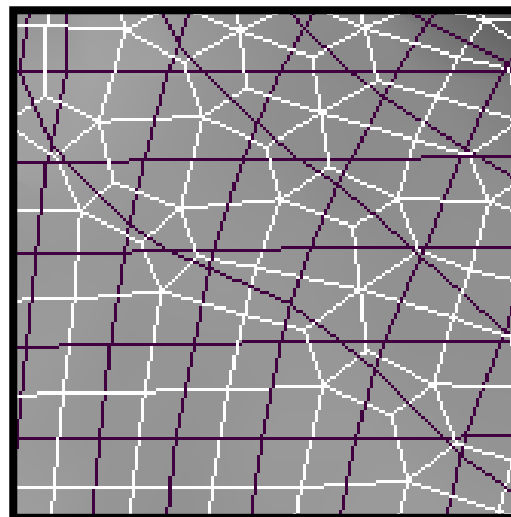


Figure 2. The edges of the MC-Patch surface are in black, the vertices of the original MC surface are at the intersections of these polygon curves. The edges of the dual surface,  $S^\diamond$ , are in white, where each one is associated with (appears to cross) an edge of the MC-Patch surface. Every vertex of the original MC surface appears to be surrounded by a quad patch of the dual surface.

---

nielson@asu.edu

In Section 2, we give the formal definition of the MC-Dual surface and details for computational algorithms. Section 3 contains several examples and applications of the MC-Dual surface. Applying the ideas of the MC-Dual to the MC-Dual itself leads to a new surface which has the same edge connectivity as the original MC-Patch surface. This is discussed in Section 4. The relationship of the present work to other research in the area is explained in Section 5.

## 2 DUAL MARCHING CUBES

In order to proceed with a more rigorous definition of the dual, it will be useful to introduce some of the basic concepts of the MC algorithm and some notation associated with it. Input to the marching cubes algorithm consists of a three dimensional array of values

$$F_{i,j,k} = F(i\Delta x, j\Delta y, k\Delta z)$$

representing samples of a function over a rectilinear grid consisting of lattice points

$$L = \{(i\Delta x, j\Delta y, k\Delta z), i = 1, \dots, N_x; j = 1, \dots, N_y; k = 1, \dots, N_z\}.$$

The cube or voxel with the diagonal from  $(i\Delta x, j\Delta y, k\Delta z)$  to  $((i+1)\Delta x, (j+1)\Delta y, (k+1)\Delta z)$  is denoted by  $B_{ijk}$ . For a given threshold value,  $\alpha$ , the MC algorithm produces a triangular mesh surface which separates the lattice points with  $F_{i,j,k} > \alpha$  from those with  $F_{i,j,k} \leq \alpha$ . The basic strategy consists of producing fragments of the surface one voxel at a time. The triangles produced for a particular voxel depend upon the case/configuration of this voxel. These cases are determined by the relationship of the value of the field function at a lattice point and threshold value. The 256 ( $= 2^8$ ) cases are grouped into a total of 23 configurations with the equivalence relationship of a rigid rotation. Representatives of these equivalence classes are shown in Figure 3.

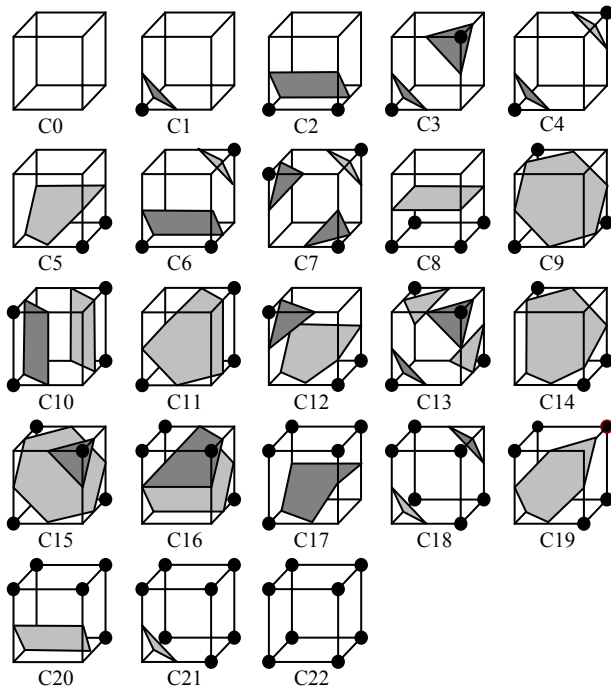


Figure 3. The configurations of the MC-Patch method.

The  $4^*$ -network consists of the edges of the MC-Patch surface. An example is shown in the middle image of Figure 1. There is considerable structure to the  $4^*$ -network in that it consists of a collection of three, mutually orthogonal planar curves. Here we assume that  $\alpha \neq F_{i,j,k}$  which guarantees that each vertex is at the intersection of exactly two of these planar polygons. Also, we assume that MC surface is without boundary so that none of its edges are in the boundary planes of the domain lattice. These are not fundamental restrictions, but simply make the discussion here simpler not having to deal with special cases.

We let  $F_j$   $j = 1, \dots, M$  denote the patches of  $S$  and

$$F_j = (V_{j_1}, V_{j_2}, \dots, V_{j_{n_j}}) \quad j = 1, \dots, M \quad (1)$$

denote the individual vertices which form the boundary of each patch. The topology of  $S$  is captured in the list of index pointers

$$(j_1, j_2, \dots, j_{n_j}) \quad j = 1, \dots, M \quad (2)$$

where each adjacent pair of indices (including cyclic pairs) indicates an edge of  $S$ . And now a simple but important observation. Since each vertex,  $V_i$ , of  $S$  lies on an edge of the lattice and since each edge of the lattice has exactly four voxels that share this edge we know that each vertex,  $V_i$ , of  $S$  has exactly four patches which touch (contain) it. This topology (neighbourhood connectivity) of the surface fragments, can be represented with a list of 4-tuples

$$(i_{00}, i_{01}, i_{10}, i_{11}) \quad i = 1, \dots, N \quad (3)$$

where this indicates that  $V_i$  is common to  $F_{i_{00}}, F_{i_{01}}, F_{i_{10}}, F_{i_{11}}$  and these four fragments are connected in a circular fashion with the two pairs of fragments  $(F_{i_{00}}, F_{i_{11}})$  and  $(F_{i_{01}}, F_{i_{10}})$  are connected diagonally as shown in Figure 4.

And now we introduce a space of MC-Patch surfaces by allowing the vertices to slide any where along their respective edges of the lattice  $L$ . We denote this collection of surfaces as  $X(\chi)$ , where  $\chi$  is an enumerated volume consisting of a distinguished subset of  $L$ . The edges joining a point in  $\chi$  to points not in  $\chi$  are the same edges containing the vertices of the MC surface. That is,

$$\chi = \{(i\Delta x, j\Delta y, k\Delta z) : F_{ijk} > \alpha\} \quad (4)$$

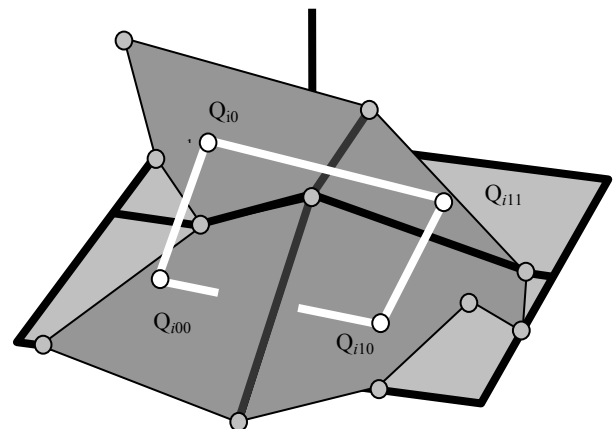


Figure 4. Four adjacent patches of the MC-Patch surface and the edges of the associated quad patch of the MC-Dual surface.

**Definition:** Let  $S$  be in  $X(\chi)$  then  $S^\diamond$  is a surface comprised of a collection of quad patches with the following properties

- 1) For each patch  $F_j$  of  $S$  there is a vertex  $Q_j$  of the dual surface,  $S^\diamond$ , lying in the interior of the voxel containing  $F_j$ .
- 2) For every vertex  $V_i$  of the the marching cubes surface,  $S$ , there is one quad patch  $P_i$  of  $S^\diamond$ . The vertices of the quad patch are the vertices that associate with each of the four patches of  $S$  that have  $V_i$  in common.
- 3) For every edge of  $S$  there is an associated edge of  $S^\diamond$ . The edge of  $S$  lies in the voxel face intersected by the associated edge of the dual surface  $S^\diamond$ . ( In the images of Figure 2, these associated edges appear to intersect.)

This definition is summarized in the following table

$S \in X(\chi)$	Dual Surface $S^\diamond \in \diamond(\chi)$
Voxel Patches: $F_j \ j=1, \dots, M$	Vertices: $Q_j = G(V_{j_1}, V_{j_1}, \dots, V_{j_{n_j}}) \ j=1, \dots, M$
Vertices: $V_i \ i=1, \dots, N$	Quad Patches: $P_i = (Q_{i_{00}}, Q_{i_{01}}, Q_{i_{10}}, Q_{i_{11}}) \ i=1, \dots, N$

Table 1: The vertices of the dual surface,  $S^\diamond$ , have the connectivity of the patches of  $S$  and the vertices of  $S$  have the connectivity of the quad patches of  $S^\diamond$ .

In a manner similar to defining  $X(\chi)$  by allowing the vertices of a specific surface to vary along its edges, we define the space of dual surfaces,  $\diamond(\chi)$  by allowing the vertices,  $Q_j$ , of the specific surface  $S^\diamond$  to be anywhere in their respective voxels.

Again, we summarize up to this point.

- 1) The topology (connectivity of vertices or patches) for both  $X(\chi)$  and  $\diamond(\chi)$  is completely determined by the enumerated volume  $\chi$  consisting of a subset of the vertices of the lattice  $L$ .
- 2) If we say that *two vertices are connected* provided there is an edge joining them and that *two patches are connected* if they have a common edge, then the following hold: The connectivity of the vertices of  $X(\chi)$  is the same as the connectivity of the patches of  $\diamond(\chi)$  and the connectivity of the vertices of  $\diamond(\chi)$  is the same as the connectivity of the patches of  $X(\chi)$ .
- 3) There is a one-to-one correspondence between the edges of  $S \in X(\chi)$  and  $S^\diamond \in \diamond(\chi)$ . The edge joining two vertices of  $S$  corresponds to the common edge to their associated quad patches.

The way we have presented and described the MC-Dual surface,  $S^\diamond$  seems to indicate that it is necessary to compute the surface  $S$  and then from this surface compute the dual surface. While for some applications, this might be desirable, it is not necessary and it is certainly possible to directly compute the dual surface. Analogous to the configuration of Figure 3, for the computation of  $S$ , we have Figure 5 for  $S^\diamond$ . Each configuration of Figure 5 indicates the number of vertices of  $S^\diamond$  each configuration produces and how these are connected to the vertices of neighboring voxels. The determination of the connectivity is through the edges. Each quad patch emanating from a vertex intersects the edge as shown in the figure. This edge is connected to the vertex of the adjoining voxel whose patch intersects this common edge. An examination of this figure will reveal that it is carefully constructed so as maintain the same face

connectivity of lattice points on the ambiguous faces ( see [11] ). With two distinguished lattice points on opposing corners, we have chosen arbitrarily, but consistently, to separate these lattice points.

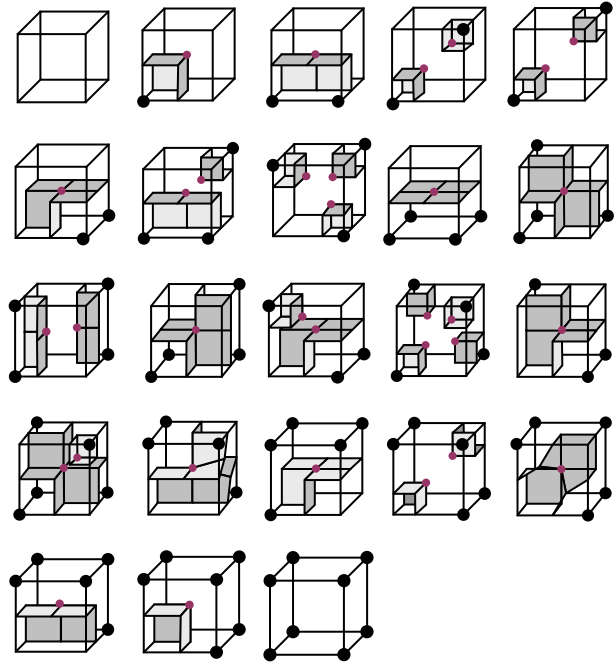
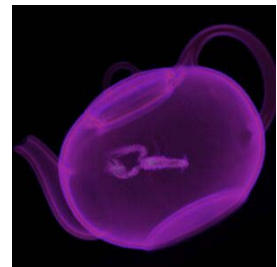


Figure 5. The configurations for the construction of the MC-Dual surface,  $S^\diamond$ .

**Simple splatting algorithm for rendering a dual surface:** If no post processing, requiring the topology information, is needed and if all that is required is to render the dual surface then it is possible to do a simple algorithm based upon simply visiting each edge of the lattice edges that has a sign change and render the patch associated with it. For simplicity, assume that the value of a dual vertex is the centroid of the midpoints of the edges associated with this vertex. We simply look at each of the four voxels which share this edge, determine which patch the edge lies in for this voxel and its configuration and compute (or look up) the value of its dual vertex. Having done this for all four voxels which share this edge, we simply then render the quad patch and move onto the next lattice edge with a sign change.

### 3 EXAMPLES OF MC-DUAL SURFACES

This first example illustrates rather typical results of comparing the original MC surface and the MC-Dual. The data set is freely available at [www.volvis.org](http://www.volvis.org). It has a field function defined over a  $256 \times 256 \times 178$  lattice and represents a CT scan of the SIGGRAPH 1989 teapot with small version of the AVS lobster inside.



In Figure 6, we compare the smooth shaded rendering of the MC surface with that of the MC-Dual surface. The big difference is in the specular reflection. The MC surface has many long thin triangles and these lead to abrupt changes and near discontinuities in the highlights. The MC-Dual surface tends to diminish this negative aspect of MC surfaces. Figure 7 illustrates this same improvement, but with a different example.

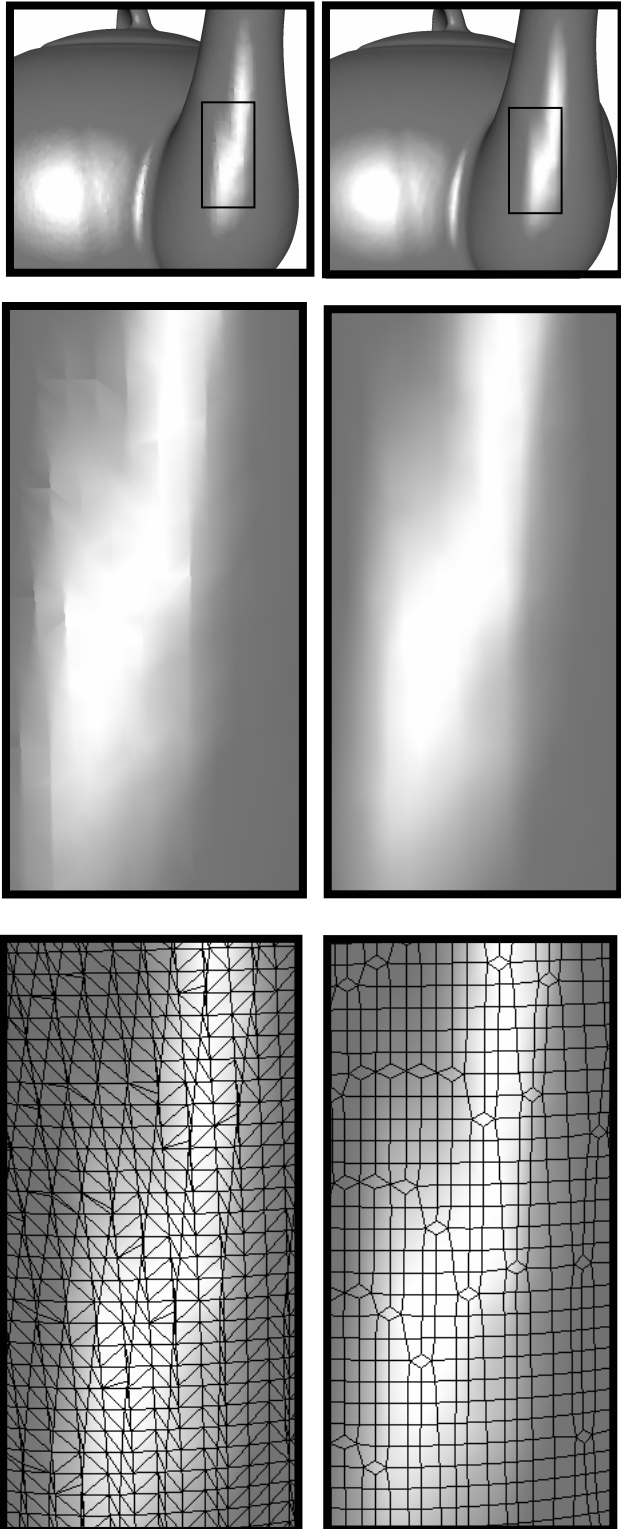


Figure 6. The top two images are the MC surface on the left and the MC-Dual surface on the right. A blow-up in the two middle images illustrates the near discontinuities of the highlights of the MC surface and the improvement gained with the MC-Dual surface. The bottom two images show the grids for these two regions of the surface.

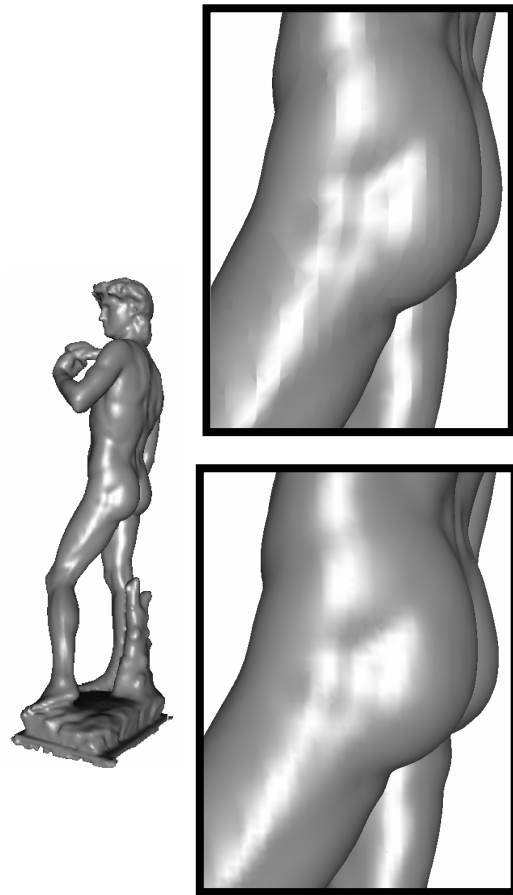


Figure 7. The top, right image is the MC isosurface and the bottom, right image is the MC-Dual surface. Note the near discontinuities of the highlights in the MC isosurface which are diminished with the use of the MC-Dual surface.

While it is possible to improve somewhat the smooth rendering of the MC surface by using alternative methods of computing estimates of the normal vectors (see [4] ) this problem of long thin triangles is really a phenomena of the uniform sampling of the field function used by the MC algorithm which is diminished by the use of the dual surface.

The next example illustrates a rather different aspect and application of the MC-Dual surface. Here we have an enumerated volume of size 512x512x200 where each voxel edge is approximately .02 inches. This data is typical of data resulting from the application of segmentation algorithms to scanned medical data, ( See Hu et al. [6] ). The original field function values,  $F_{ijk}$  (which played a key role in the segmentation process) are no longer relevant for isosurface or rendering computations since there is **no** threshold value,  $\alpha$  , so that

$$\chi_{foot} = \{ (i\Delta x, j\Delta y, k\Delta k) : F_{ijk} > \alpha \}.$$

Without additional information or assumptions, we can obtain a rendering of this enumerated volume by displaying the separating midpoint surface. We show this surface and a zoom-in in Figure 8. The midpoint surface is rather blocky, making it difficult to discern shape information. The dual is also a separating surface that makes no assumptions about the values of the field function, but, as is shown in the bottom image of Figure 8, is much smoother and reveals much better shape information.

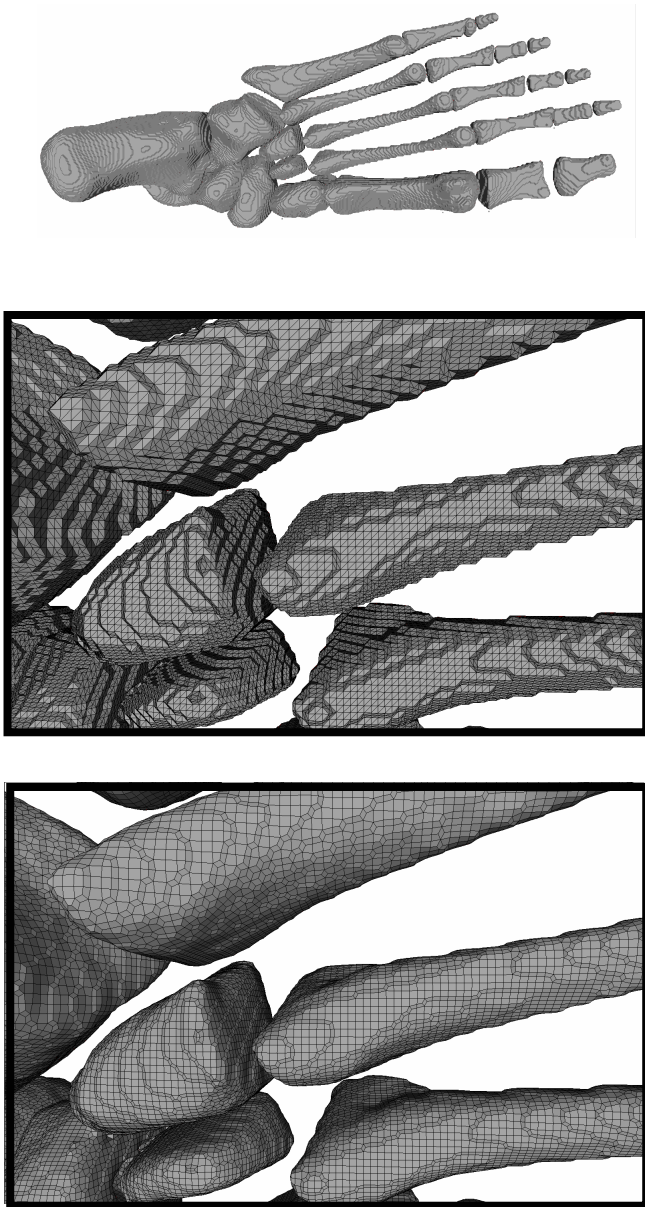


Figure 8. The top image and middle zoom-in illustrate an enumerated volume  $\chi_{foot}$  with a midpoint surface. The MC-Dual, which is also a separating surface that tends to be smoother, is shown in the bottom image.

#### 4 DUAL OF THE DUAL

In this section, we describe a specific mapping from a MC-Dual surface  $R \in \diamond(\chi)$ , back to a MC-Patch surface,  $R^+ \in X(\chi)$ . For each edge of the lattice with a sign change there is an associated quad patch of  $R$ . We define  $R^+$  to be the surface of  $X(\chi)$  whose vertices are the intersections of the quad patches of  $R$  with the edges of the lattice  $L$ . For this we will require that whatever quad patch is used, it must have the property that it always intersects its associated edge of the lattice. For the examples presented here, we use a quad patch comprised of two triangles. There are potentially two possible ways to triangulate a quadrilateral. We

consider the projection of the quad patch boundary onto the plane perpendicular to the edge associated with the quad patch. See Figure 9. If this planar quadrilateral is convex then either diagonal is acceptable. If it is not, then one of the points is in the triangle formed by the other three. This point is joined to its opposing point to form the diagonal. The intersection point is then computed using barycentric coordinates. Under some circumstances and modifications, it is also possible to use a bilinear quad patch, but we forego the details of this now.

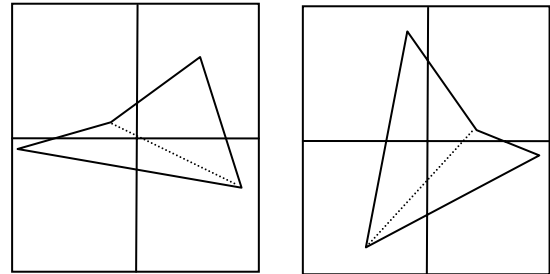


Figure 9. The definition of the two-triangle quad patch requires the choice of the diagonal based upon the footprint configuration.

**Definition:** Let  $S \in X(\chi)$ , then the *Dual-of-the-Dual* is

$$S^v = (S^\diamond)^+$$

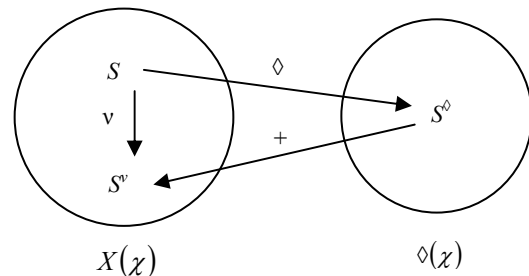


Figure 10. The Dual-of-the-Dual operator,  $v : S \rightarrow S^v$ .

In the case of the centroid and two-triangle quad patch there are some smoothing effects of  $v$ -operator which are illustrated by polygon version example of Figure 11.

We denote the iterative repetition of this operator by  $(S^v)^v = S^{2v}$ , and so  $(S^{nv})^v = S^{(n+1)v}$ . Iteration of the  $v$ -operator leads to a sequence of surfaces possibly converging to a limiting surface

$$\text{Lim}_{n \rightarrow \infty} S^{nv} = S^{\infty v}$$

where, we call this limiting surface,  $S^{\infty v}$ , the *fixed-point shroud of  $\chi$* . This is called a fixed-point surface because the  $v$ -operator does not affect this surface. That is,

$$(S^{\infty v})^v = S^{\infty v}.$$

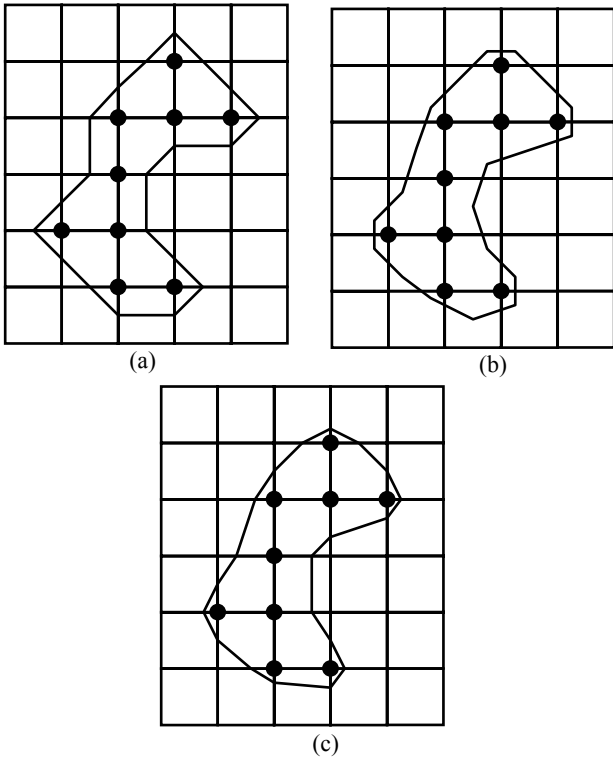


Figure 11. Image (a) is the midpoint curve and (b) is the dual curve. The dual-of-the-dual is shown in image (c). The  $v$ -operator maps (a) to the smoother (c).

An example of a Fixed-Point Shroud is shown in Figures 12. In Figure 13, we show results for a random initial separating surface.

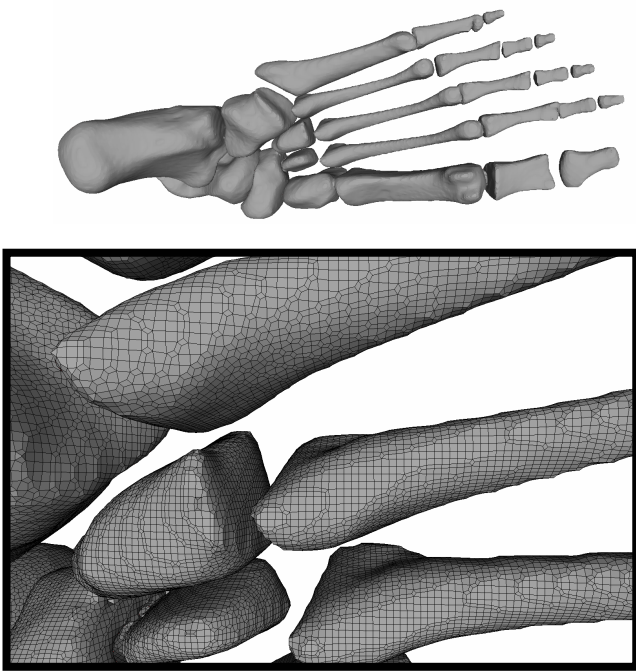


Figure 12. The upper image is the Fixed-Point Shroud,  $S^{\infty v}$ , for the enumerated volume of the data of Figure 8. The lower image is a zoom-in of the dual of this surface,  $(S^{\infty v})^{\vee}$ .

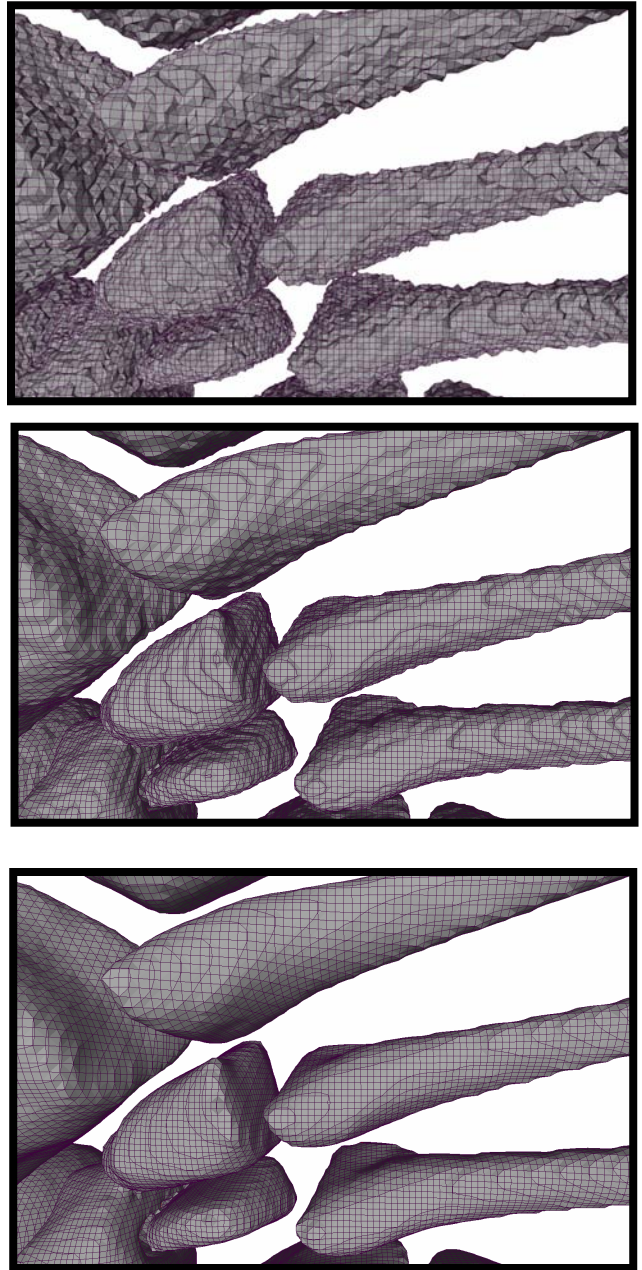


Figure 13. Top image utilizes random values on the edges of the lattice of the enumerated volume as an initial surface. The Dual-of-the-Dual of the random surface is the middle image and the bottom image is the result of 13 iterations of the  $v$ -operator applied to the random initial surface which has nearly converged to the Fixed-Point Shroud,  $S^{\infty v}$ .

In Figure 14, we show some results of the present method applied to segmented MRI data (see Hu et al. [6]). Rather than use a zoom-in, we have used a down-sampled version of the actually data set so that the effects of the  $v$ -operator are more apparent.

## 5 SUMMARY AND REMARKS

### 5.1 Relation to Other Work in the Area

In this section, we discuss how the present techniques relate to others in the literature. We first note that meshes dual to the general triangular mesh produced by the MC algorithm are really quite different from the dual meshes we have described here which are dual to the MC-Patch surfaces. This includes the methods of Ohtake and Belyaev [14] which is motivated by the observation that a tangential surface element that is tangential to an implicit surface has a better chance to approximate it than ones that interpolate to it. They use the dual mesh of the general triangular mesh produced by the MC method and additional subdivision to gain better approximations to features.

The cuberille method was first described by Herman and Liu [5] and later Chen et al. [1] discussed methods for estimating normals for displaying these surfaces. The cuberille method is described in terms of voxels belonging to objects and not lattice points as we have used here, but considering the voxels with lattice points being the centers of our voxels we have an equivalent context. Within this context, the boundary surfaces of the cuberille method can be computed per voxel using the scheme indicated in Figure 15. Gaubin [15] has noted that the resulting surfaces are not proper two-dimensional manifolds in that several quad patches can share an edge and mentions ( see Kalvin [8] ) the possibility of regularizing these surface to manifolds by inserting vertices and duplicating edges with a shrinking type of approach. This would be different than the table-look-up technique we have described here and could possibly be viewed as shrinking the surface fragments of Figure 14 to those of Figure 5.

The edges of the cuberille produced surfaces are subsets of the edges of SurfaceNets ( see Frisken [3] ) which include one vertex per surface cube. A surface cube of this method is defined to be 8 voxel neighbors not all of the same binary value indicating inclusion of the segmented object. Vertices are joined across cube faces and a spring model is used to compute the actual final location of each vertex. Subsequently triangles join the vertices leading to surfaces that can be rendered. A related method is that of Whitaker [16] which he describes as a “reformulation of the technique of constrained elastic surface nets” and level sets are used to estimate surfaces of minimal area.

Ju et al. [7] describe their method with: “This method is an interesting hybrid of the EMC method and the SurfaceNets method. It uses the EMC method’s feature vertex rule for positioning all vertices of the contour while using the SurfaceNets method to determine the connectivity of these vertices.” Here, EMC refers to the method of Kobbelt et al. [9].

In some applications, for example where the rendering of the surface is the only aspect of interest, the lack of the manifold property ( of the three previously mentioned methods ) may not be an important problem, but where surface intrinsic properties are needed ( e. g. normals, curvature, etc. ) or where any post geometric processing of surfaces is done ( simplification, multiresolution, etc. ) then the manifold property is important. The separating surfaces described here have this manifold property. This comes at the expense of dealing with more than one vertex per voxel. If the configurations C6, C7, C10, C12, C13, C15, and C18 never occurred, then a much simpler approach could be taken, but these configurations do occur in most applications. We have found that typically these configurations comprise about 1.3% of all configurations C1 to C22.

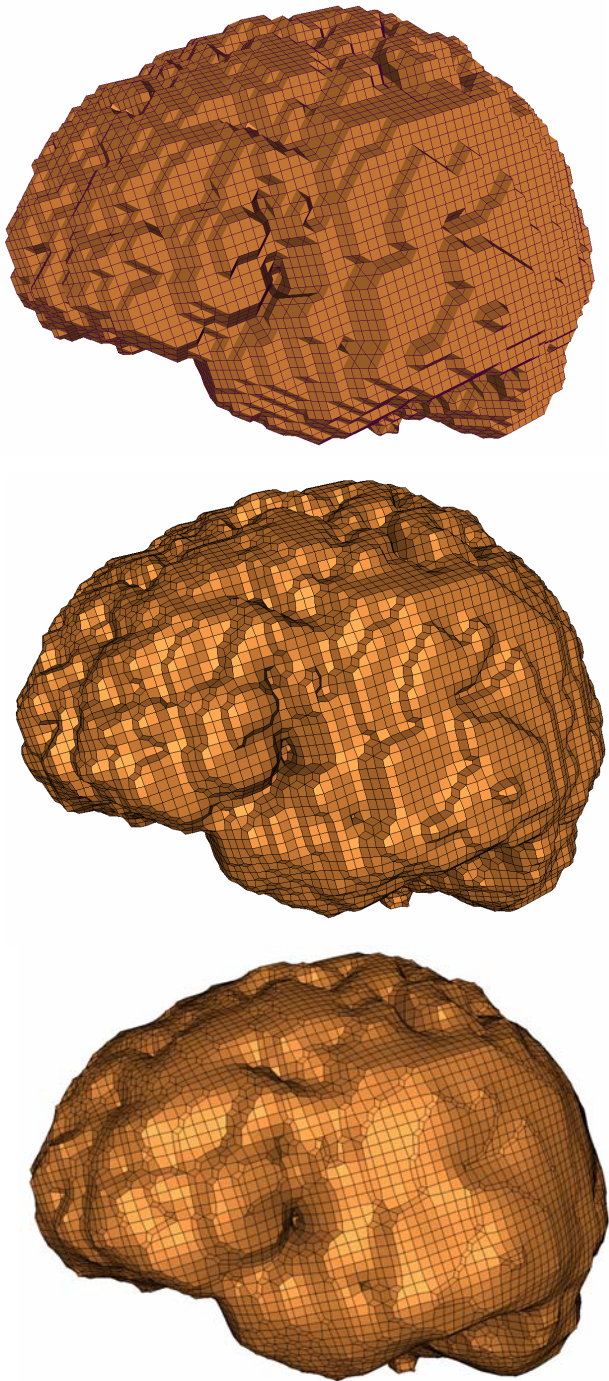


Figure 14. The top image is the midpoint separating surface for an enumerated volume which results from a segmentation algorithm ( see Hu et al. [6] ) applied to MRI data. The middle image is the MC-Dual surface of the midpoint surface and the bottom image is the dual of the Fixed-Point Shroud. We have used a down-sampled version of the original data for this example so the effects of the new method are more apparent.

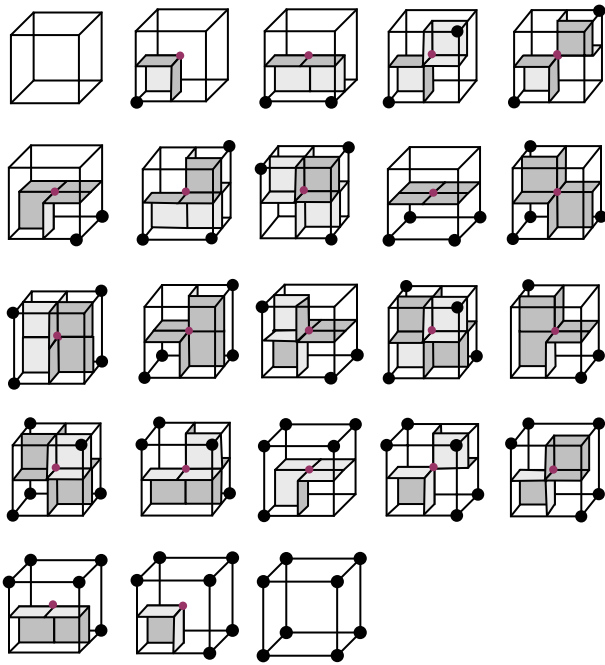


Figure 15. The connectivity of the quad patches for the cuberille method.

## 5.2 The Specific Choices for the Dual Points and the Quad Patches

We have presented our new method as a general framework and have not been specific about certain aspects of the process. For the examples presented here, the vertices of the MC-Dual were simply taken as the centroids of the vertices of the associated patch. How to define and compute the MC-Dual vertices is a wide open research topic with the possibility of variety of new techniques based upon the application domain and/or the information that might be available (e. g. Hermite data). Incorporating the ideas of (the geometry of) surface nets into this context would be interesting. We have investigated some techniques which produce dual surfaces with certain specific Gaussian curvature characteristics and we will report on this in the near future. We are also investigating techniques that will make the  $v$ -operator the identity operator (or nearly). That is, the vertices of the quad patches are selected so as to yield specified intersection points on the lattice edges. Also, the specific choice of the quad patch for the MC-Dual and its influence on the dual-of-the-dual is an open question with choices having effects on the overall characteristics of the Fixed-Point Shroud. Here we used the simple two-triangle quad patch and alluded to the use of a bilinear patch. Patches of higher order continuity would be interesting and potentially useful. In the case where the centroid and two-triangle patch are used, it is easy to see that a new vertex of the dual-of-the-dual is a convex combinations of its star vertices. This property tends to force a number of the patches of the Fixed-Point Shroud to be degenerate with vertices at points of the lattice. Different techniques for choosing the dual vertices will, of course, lead to different results which make this whole topic rather interesting.

## 5.3 Additional Remark

If a configuration C16 or C19 ( see Figure 3 and Figure 5 ) share a common ambiguous face, then we get a dual surface where two edges become coincident. The surface is still a two manifold in that no edge is shared by more that two quad patches. This can be viewed as a situation where a topological tunnel has geometrically collapsed. This phenomenon is a result of the decision to be consistent with the MC topology given in Figure 3 to always separate the opposing vertices on the ambiguous faces.

## Acknowledgments

We wish to acknowledge the support of the Office of Naval Research (N00014-97-1-0243 & N00014-00-1-0281), the National Science Foundation ( NSF IIS-9980166 & ACI-0083609) and DARPA ( MDA972-00-1-0027). Thanks to R Holmes, J. Hu, A. Huang, Y. Lu and M. Phielipp, for their help.

## REFERENCES

- [1] L. Chen, G. Hermann, R. Reynolds and J. Udupa. Surface shading in the cuberille environment, *Computer Graphics and Applications*, 5:33-42, 1985.
- [2] D. Cohen-Or, A. Kadosh, D. Levin & R. Yagel. Smooth boundary surfaces from binary 3D datasets, in: *Volume Graphics*, M. Chen, A. E. Kaufman, R. Yagel (eds.), pp. 71-78, Springer, 2000.
- [3] S. Frisken. Constrained elastic surface nets: generating smooth surfaces from binary segmented data, *MICCAL*, pages 67-76, 1999.
- [4] A. Huang and G. M. Nielson. A comparison of weighted average methods for computing normals for marching cubes isosurface, *Proceedings of Vision, Mathematics and Visualization*, pages 399-406, 2003.
- [5] G. Herman and H. Liu. Three dimensional display of human organs from computed tomograms, *Proc. Comp. Graph. Im.*, 9:1-21, 1979.
- [6] J. Hu, A. Razdan, G. Nielson, G. Farin, D. Page and D. Capco. Volume segmentation using Weibull E-SD fields, *Transactions on Visualization and Computer Graphics*, 9:320-328, 2003.
- [7] T. Ju, F. Lasasso, S. Schaefer and J. Warren. Dual contouring of Hermite data, *Proceedings of SIGGRAPH 2002*, pages 43-52, 2002.
- [8] A. Kalvin. Segmentation and surface-based modeling of objects in three-dimensional biomedical images, PhD Thesis, New York University, New Your, March 1991.
- [9] L. Kobbelt, M. Botsch, U. Schwanecke and H. Seidel. Feature sensitive surface extraction from volume data, *Proceedings of SIGGRAPH 2001*, pages 57-66, 2002.
- [10] W. Lorensen and H. Cline. Marching cubes: A high resolution 3D surface construction algorithm, *Proceedings of SIGGRAPH 1987*, pages 163-169, 1987.
- [11] G. M. Nielson and B. Hamann. The asymptotic decider: Resolving the ambiguity in marching cubes, *Proceedings of Visualization 1991*, pages 83-91, 1991.
- [12] G. M. Nielson. On marching cubes, *Transactions on Computer Graphics and Visualization*, 9:283-297, 2003.
- [13] G. M. Nielson, G. Graf, A. Huang, M. Phliepp and R. Holmes. Shrouds: Optimal separating surfaces for enumerated volumes, *Proceedings of VisSym 2003*, Eurographics Association, pages 75-84, 2003.
- [14] Y. Ohtake and A. Belyaev. Dual/primal optimization of polygonized implicit surfaces with sharp features, *Journal of Computing and Information Science in Engineering*, 2:23-45, 2002.
- [15] T. Gaubin. BLIC: Bi-level isosurface compressions, *Proceedings of Visualization 2002*, pages 451-459, 2001.
- [16] R. Whitaker. Reducing aliasing arefacts in iso-surfaces of binary volumes, *Proceedings of Symposium on Volume Visualizaton*, ACM Press, pages 22-32, 2000.